Independent origins of spicules reconcile the evolutionary history of sponges

Maria Eleonora Rossi[1,2], Nathan James Kenny[2,3], Mattia Giacomelli[1], Joseph N. Keating[1], Sandra Álvarez-Carretero[1], Astrid Schuster[4], Paco Cárdenas[5,6], Sergi Taboada[2,7,8,9], Vasiliki Koutsouveli[2,10], Philip Donoghue[1*], Ana Riesgo[2,7,9*] and Davide Pisani[1*]

1 - Bristol Palaeobiology Group, School of Earth Sciences, University of Bristol, Life Sciences Building, Tyndall Avenue, Bristol BS8 1TH, UK

2 - Life Sciences Department, The Natural History Museum, London SW7 5BD, UK

3 - Biochemistry Department, School of Biomedical Sciences, University of Otago, Dunedin, Aotearoa New Zealand

4 - Department of Biology, University of Southern Denmark, Campusvej 55, Odense M 5230, Denmark

5 - Pharmacognosy, Department of Medicinal Chemistry, Uppsala University, Husargatan 3, Uppsala 751 23, Sweden

6 - Museum of Evolution, Uppsala University, Norbyvägen 16, Uppsala 752 36, Sweden

7 - Department of Biodiversity and Evolutionary Biology, National Museum of Natural Sciences (CSIC), c/José Gutiérrez Abascal 2 28006 Madrid, Spain

8- Departamento de Biodiversidad, Ecología y Evolución, Facultad de Ciencias, Universidad Complutense de Madrid, Madrid, Spain

9 - Departamento de Ciencias de la Vida, EU-US Marine Biodiversity Group, Universidad de Alcalá, Alcalá de Henares, Spain

10 - Division of Marine Ecology, Marine Evolutionary Ecology, GEOMAR Helmholtz Centre for Ocean Research Kiel, Kiel, Germany

**Corresponding authors: Philip C.J. Donoghue (Phil.Donoghue@bristol.ac.uk), Ana Riesgo (anariesgogil@mncn.csic.es), and Davide Pisani (davide.pisani@bristol.ac.uk).*

Sponges (Porifera) are highly effective ecosystem engineers, playing a critical role in global biogeochemical processes, including the nitrogen, carbon, and silica cycles. Because of that, they have been closely linked to the evolution of Earth's environments. However, determining the evolutionary history of sponges has posed challenges. Molecular divergence times have pointed to a Tonian or Cryogenian origin for sponges. This contrasts with the oldest unequivocal fossil evidence for sponges, consisting of isolated siliceous spicules from the latest Ediacaran, resulting in a 150-million-mismatch with molecular clock estimates. This mismatch may arise because molecular clock estimates are inaccurate, the fossil record is incomplete, and/or the fossil record has been misinterpreted in the calibration of molecular clock analyses or some combination of the above. To resolve the deep evolutionary history of sponges we compiled an extensive phylogenomic dataset of sponges, revised fossil calibration evidence to derive a new phylogeny and timescale for sponge evolution, and investigated the evolutionary origin of the sponge spicules. Our results confirm that sponges include two main lineages: Silicea (Hexactinellida plus Demospongiae) and Calcarea plus Homoscleromorpha. Our molecular clock analyses identify an early Ediacaran estimate for the crown ancestor of sponges. Our study of spicule evolution shows that neither the last common sponge ancestor, nor the last common ancestors of Silicea and (Calcarea plus Homoscleromorpha) possessed siliceous spicules, which independently evolved four times in sponges: once in Hexactinellida, twice in Demospongiae, and once in Homoscleromorpha. Furthermore, diversification rate analyses demonstrate that the origin of spicules did not align with species radiations within the phylum. Our dating analyses substantially reduce the mismatch between molecular clock estimates for the antiquity of sponges and their fossil record. Our study of the evolutionary history of siliceous spicules reconciles the remaining difference as a consequence of crown-sponges primitively lacking siliceous spicules. As such we demonstrate the power of combining molecular and palaeontological approaches to establishing evolutionary timescales which together allow us to calibrate genome evolution to geological time and read evolutionary history within the gaps in the fossil record.

Molecular clock estimates and fossil biomarkers suggest that sponges diverged in the Tonian or Cryogenian[1–5] anticipating a deep Neoproterozoic appearance of sponge fossils. However, while fossils from the Tonian, Cryogenian and Ediacaran have been claimed to represent early sponges, this evidence is difficult to interpret[6]. For example, C_{30} steranes interpreted as evidence for Cryogenian demosponges – that is 24-ipc and 26-mes[3], can also be interpreted as diagenetically altered C_{29} sterols from chlorophyte algae[7]. Arsenopyrite crystals aggregates, and other fragmentary structures have been misinterpreted as siliceous sponge spicules[8] while scanning of Tonian fossils that resemble sponge-like ostia[9], and of the ~600 Ma old *Eocyathispongia qiania* (that was originally interpreted as

65 an adult asconoid sponge), demonstrated that they lack the internal structures expected in sponges[10].
66 Accordingly, there is a minimal mismatch of 150 Ma between molecular estimates of divergence times
67 and fossil evidence for the origin of the sponges, with the earliest, unambiguous, sponge fossils being
68 represented by loose, late Ediacaran ~543 Ma, siliceous spicules [6,11,12].

69 Three sponge lineages make spicules out of silicic acid (Hexactinellida, Homoscleromorpha
70 and Demospongiae). The fourth lineage, Calcarea, makes spicules with calcite. Calcite preservation
71 potential decreases with age, and it is possible that Neoproterozoic sponges were calcified. However,
72 even assuming that the earliest sponges might have been calcareous, the oldest fossil sponges are
73 represented by siliceous spicules, and the evolution of calcareous spicules is not relevant to
74 understand the evolution of siliceous sponges. For this reason, we will not consider calcite spicule
75 evolution any further in this study. Silica is chemically stable under low-temperature and high-
76 pressure conditions[6]. If siliceous spicules existed in the Neoproterozoic we should expect to find them.
77 Four hypotheses have been proposed to explain the absence of Neoproterozoic siliceous spicules: (1)
78 Molecular clock estimates of sponge divergence times are not reliable, putative sponge biomarkers
79 are not diagnostic of sponges, and sponges evolved in the early Cambrian[13]; (2) Sponges emerged in
80 the Neoproterozoic but early sponge spicules were unmineralized and had low preservation
81 potential[12]; (3) Neoproterozoic ocean geochemistry and/or depositional regimes were unfavourable
82 for the preservation of mineralized spicules[14,15]; (4) Spicules were not present in the Last Common
83 Ancestor (LCA) of sponges and in early sponges more broadly. If this was the case, then siliceous
84 spicules must have independently evolved multiple times during sponge history[16].

85 Here we test alternative hypotheses of the age of sponges and the origin of siliceous spicules
86 using phylogenetic analyses, divergence time estimation, ancestral state estimation (ASE), and
87 diversification rate shift analyses. We then interpret these results to generate an integrative history
88 of sponge evolution. We first constructed a time-calibrated phylogenomic tree based on 70
89 transcriptomes, 12 of which were newly sequenced. We tested the effect of competing calibration
90 strategies on the timescale of sponge evolution and used ASE to elucidate siliceous spicule evolution.
91 The results of our analysis indicate that sponges evolved in the early Ediacaran (~608 Ma) and that the
92 crown ancestors of all extant sponges and of the silicean (i.e. Hexactinellida plus Demosponges)
93 sponges did not possess silicified spicules. Spicules evolved independently in Homoscleromorpha,
94 Hexactinellida and Demospongiae. In Demospongiae, the most biodiverse sponge lineage, siliceous
95 spicules emerged in the stem of Heteroscleromorpha plus Haplocleromorpha (the spiculated
96 demosponge lineages) after they diverged from the clade composed of Keratosa and Verongimorpha
97 (the aspiculated demosponge lineages). One further independent (convergent) origin of siliceous
98 spicules is observed within the aspiculated sponges, where the Verongimorph genus *Chondrilla*

possess siliceous spicules. We performed a focal study, using diversification rate shift analyses, on the demosponges (the most diverse sponge lineage), and found only two potentially significant diversification shifts. These happened in Poecilosclerida and the clade comprised of Axinellida plus Bubarida, both of which are spiculated lineages deeply nested within the Heteroscleromorpha, that significantly postdate the emergence of siliceous spicules. Siliceous spicules emerged late in sponge evolution, and they do not seem to have played a significant role in the diversification of the Demospongiae. While our results imply that the emergence of siliceous spicules in the fossil record cannot be used as a proxy for the age of Porifera, our new revised estimate of divergence time, in combination with our study of the evolution of siliceous spicules, *de facto* reconcile the sponge fossil record with molecular estimates of divergence times.

Results

Phylogenomic and molecular divergence time analyses

Phylogenomic analyses (see Fig S1—S3) recover Silicea (Hexactinellida plus Demospongiae) as the sister of Calcarea plus Homoscleromorpha. In Demospongiae, we retrieve the aspiculated Keratosa and Verongimorpha to form the monophyletic sister group of the spicule-bearing Heteroscleromorpha. Relationships in our phylogeny mostly show full support. The only exception is the relationships between Suberitida, Poecilosclerida, Clionaida, and Tethyida in Heteroscleromorpha, where Suberitida clusters either with Poecilosclerida (in the Bayesian Analyses – BA) or with a Clionaida plus Tethyida (Maximum Likelihood – M; and Astral-based Coalescent analyses – CA; see Fig S1—S3).

Molecular divergence times (Fig. 1) were inferred for the Bayesian phylogeny (Fig. S3), using 12 fossil constraints to calibrate the ages of major sponge clades (see nodes highlighted with red circle in Fig. 1 and supplementary material for detailed descriptions of all 12 calibrations). We calibrated the root to have a hard minimum of 574 Ma and a soft maximum of 609 Ma. The fossil minimum is based on the earliest occurrence of *Charnia masoni*, in the Drook Formation of Mistaken Point, Newfoundland[17], while the maximum is based on the Lantian biota of South China which contains a diversity of macrofossils but no credible metazoans[18]. A uniform prior was used for this calibration, implying that we maintain an agnostic view of where the root of our phylogeny might lie between these constraints. The maximum on the root node is soft, with 2.5% of the probability density falling outside of the 574–609 Ma interval, on the deep side of the distribution. Accordingly, our analyses did not preclude the inference of a deeper age for the origin of sponges. Eumetazoa was assigned a hard maximum of 573 Ma. This value was empirically identified to avoid truncation problems in MCMCTree (see Methods for details) and a soft minimum of 561 Ma based on age of Bed B in the Bradgate

Formation from which the earliest crown-eumetazoan, *Auroralumina attenboroughii*, was recovered[19,20]. While it was possible to establish minimum constraints for the remaining sponge calibrations, it was not possible to justify maximum constraints based on palaeontological, biogeographic or geological evidence. The sponge fossil record, at least in terms of records that can inform calibrations for molecular clock analyses, is based on sites of exceptional fossil preservation. As such, we have no prior expectation of whether the earliest records of various sponge clades (Details in Supplementary Information) represent close approximations of true clade ages. Cauchy distributions with a heavy-tail (see methods) were used for these calibrations, to reflect the lack of knowledge for maxima.

Two calibration strategies were used. First, we performed analyses where the oldest known siliceous spicule was used to constrain the crown Heteroscleromorpha clade. We refer to this calibration strategy as the Spiculated Demosponges Node (SDN) strategy. We then performed an analysis where the same calibration was used to calibrate the root of Porifera – Spiculated Porifera Node (SPN) strategy. These calibration strategies were implemented to reflect competing interpretations of the fossil record of siliceous spicules. Under the SDN strategy, early siliceous fossil spicules are assumed to represent remains of spicule-bearing demosponges, as suggested by the morphological similarity between the oldest classifiable siliceous spicules[7,21] and those found in living demosponges. Under the SPN strategy, siliceous spicules are assumed to have been present in the last common ancestor of Porifera, with the spicule fossil record providing a bound on the origin of sponges. We visualised the joint time priors (Fig. S4), to make sure that there was no major disagreements between our specified and effective priors (see Fig. S5).

We then performed molecular clock analyses, under both calibration strategies (SDN and SPN), using both the Autocorrelated Rates (AR)[21,22] relaxed molecular clock model, and Independent rates (IR)[23,24] relaxed molecular clock model, and the Independent Rates (IR)[22,23] relaxed molecular clock model. For each analysis (a total of four SDN-AR; SDN-IR; SPN-AR and SPN-IR), we run six independent chains. We checked for convergence and dismissed results from chains that did not converge, Fig. S6 and Methods for details. Under the SDN strategy, three chains converged (and were therefore retained) under both the AR and IR models (Table S1).

Results inferred using the two clock models and different calibration strategies did not differ significantly, and here we only discuss results from the SDN-IR analysis. Results from all other analyses can be seen in Supplementary Results (Fig. S7 to Fig. S9; Table S3-S4). Our SDN-IR analysis inferred the last common metazoan ancestor to have emerged between 616.9-605.9 Ma (early Ediacaran) (Table 1). Similarly, the sponge LCA was dated to 615.3–601.3 Ma (early Ediacaran). Crown-group Silicea (Hexactinellida + Demospongiae) was estimated at 591.3–570.3 Ma (middle Ediacaran),

Lyssacinosida (within Hexactinellida) at 457.3–445 Ma (late Ordovician), and the last common ancestor of Calcarea and Homoscleromorpha at 566.5–487.6 Ma (late Ediacaran to late Cambrian). Homoscleromorpha was estimated to have originated at 429.1–228.6 Ma (middle Silurian – late Triassic), and Calcarea at 351.7–213.89 Ma (early Carboniferous – late Triassic). The last common demosponge ancestor is estimated at 559.17–536.53 Ma (late Ediacaran – early Cambrian), and the last common ancestor of the non-spiculated Verongimorpha and Keratosa at 521.85–430.44 Ma (early Cambrian – middle Silurian). The last common ancestor of the spicule-bearing demosponges (Heteroscleromorpha) is estimated to have existed between 521.97–515.05 Ma (middle Cambrian), and the last common ancestor of the Haplosclerida was inferred at 403.84–246.54 Ma (early Devonian – middle Triassic). The last common ancestor of the rest of the Heteroscleromorpha was inferred to have existed 503.17–412.61 Ma (middle Cambrian – early Devonian). Within Heteroscleromorpha, the freshwater Spongillida separated from the marine Scopalinida at 424.69–325.85 Ma (late Silurian – late Carboniferous), while the three most speciose heteroscleromorph lineages (Tetractinellida, Poecilosclerida and Spongillida) diverged, respectively, 299.37–231.07 (early Permian – late Triassic), 236.53–199.74 Ma (late Triassic – early Jurassic), and 123.21–71.52 Ma (Cretaceous).

Ancestral state estimation of siliceous spicules

Ancestral state estimation (ASE) results support the absence of spicules at the root of Porifera. Absence is the most likely state irrespective of the calibration strategy used, ASE model used, or whether characters were treated as independent or amalgamated. Absence of spicules at the root of Porifera is strongly supported by the four-state model and the amalgamated Structured Markov Model (SMM) when averaged using BIC (Fig. 2). Results are more ambiguous when using the two-state model, or if any model is averaged using uncertainty (see Fig. S10-S11). However, in all these cases, absence of spicules at the root of Porifera remains the most probable state (see Fig. S10-S11). The dating method had little effect on the ASE results. Using the SMM we were able to accommodate the hierarchical nature of the data, the results amalgamated with the BIC (Fig. 2) show that the LCA of Silicea most likely did not have mineralised siliceous spicules and that siliceous spicules independently evolved three times in Silicea and once in Homoscleromorpha. In Silicea, siliceous spicules evolved once in the stem hexactinellid lineage, once in the lineage leading to Heteroscleromorpha, and once in the verongimorph genus *Chondrilla*. Based on our sponge timetree, we can conclude that demosponge spicules emerged in a ~31 Ma interval between 548 and 517 Ma (Fig. 1), in accordance with the fossil record. In Homoscleromorpha, silicified spicules were only acquired by the Plakinidae, after the divergence from Oscarellidae in the Carboniferous. When the results are amalgamated using raw uncertainties, the sponge and Silicea LCAs are still reconstructed to have been, most likely,

without spicules. Similarly, an independent origin of siliceous spicules in Homoscleromorpha continues to be supported (see Fig. S11).

Diversification events in Silicea

Because three independent origins of silicified spicules are inferred in Silicea, we tested the effect of the origin of silicified spicules in sponge evolution inferring diversification rates shifts in this lineage. To achieve this goal, following DeBiasse et al.[25], we first generated a megaphylogeny of Silicea performing a constrained ML analysis of 807 *Cytochrome c Oxidase 1* (COI) barcodes, using our phylogenomic tree (Fig. 1 and S3) as a backbone constraint (see Methods for details). The megaphylogeny was then dated (see Methods) and used to perform diversification analyses using BAMM[26] and Medusa[27] (Fig. S12 and Table S5; see Methods for details). BAMM identified two diversification shifts in both the AR and IR timetrees (Table S6). In the AR timetree, rate shifts are identified on the branches leading to the Axinellida plus Bubarida, and at the origin of the Poecilosclerida (Fig. 3A). In the IR topology, rate shifts were inferred on the branch leading to Hexactinellida, and again on the branch leading to the LCA of Axinellida and Bubarida (Fig. 3C). Using Medusa diversification rate shifts were identified in the branches leading to Axinellida plus Bubarida and Poecilosclerida for both models (Fig. 3B-D), with the IR tree also identifying a shift in Dictyoceratida (Fig. 3D).

Discussion

Mineralized sponge spicules are not homologous

Our phylogenomic analyses confirmed that sponges are split into two fundamental lineages, Calcarea plus Homoscleromorpha, and Demospongiae plus Hexactinellida (Silicea). As suggested by previous studies[28], within Demospongiae, we recovered the monophyly of Keratosa, Verongimorpha, and Heteroscleromorpha. Consistent with previous phylogenomic and mitochondrial genomic studies[28,29], we found the spicule-less Keratosa and Verongimorpha to be each other's sister lineage, and the spicule-bearing Heteroscleromorpha are found to represent the sister of Keratosa plus Verongimorpha. A long-standing problem in Demospongiae phylogeny is that of the relationships of Bubarida[10]. Our tree recovers Bubarida as the sister of (Agelasida+Plymastiida+Tethyida+Clionaida+Suberitida+Poecilosclerida). However, we could not resolve the relationships of Suberitida with reference to Clionaida, Tethyida, and Poecilosclerida, see Fig. S1-S2.

All our molecular clock analyses recovered an Ediacaran origin of sponges and a Cambrian origin for the spicule bearing demosponges (Heteroscleromorpha). Taxon sampling does not allow us

234 to date the origin of Hexactinellida. However, the oldest known Cambrian and latest Ediacaran sponge
235 spicules do not bear resemblance to the hexactinellid spicules, due to the different shape of the axial
236 filament, which always has a square cross-section in Hexactinellida, a shape never found in
237 Demospongiae or in the oldest fossil spicules. Our ASEs inferred that siliceous spicules were absent
238 from the root of sponges, Silicea, and Homoscleromorpha, suggesting instead independent origins for
239 this trait in the stem Hexactinellida, within Homoscleromorpha (in the stem Plakinidae), and in
240 Demospongiae (in the stem Heteroscleromorpha) and in the verongimorph genus *Chondrilla*.
241 Cambrian siliceous spicules are comparable to those of extant spicule-bearing demosponges [15,30], and
242 given also the results of our ASE analyses, we can only conclude that latest Ediacaran and Cambrian
243 siliceous spicules were from species belonging to total group Heteroscleromorpha plus
244 HaploslceromorpHa, postdating the deepest divergences in Porifera.
245 To better understand whether siliceous biomineralisation could have evolved multiple times
246 independently, we turned to biochemical evidence. It has been shown that silica biomineralisation is
247 the result of different processes in different sponge lineages[16,31–33]. Demosponges use silicateins
248 enzymes[34–36] and hexactinellids use glassin, perisilin, and hexaxillin with the organic part of the spicule
249 (the axial filament) having different composition[33]. *In vitro* experiments in demosponges, particularly
250 with *Suberites domuncula*, have demonstrated that the self-assembly of silicateins is a fundamental
251 step in the process of spicule biogenesis. This process creates scaffolds where silica is immediately
252 deposited[36]. The implication is that, at the least in demosponges, spicules seem to only develop as
253 biomineralised structures, precluding the possibility that siliceous spicules could have evolved from
254 organic (non biomineralised) ones[12,33].
255
256 **The appearance of silicified spicules did not drive diversification events**
257 Sponges are globally distributed and comprise ~9,600 species[37]. In terms of biodiversity,
258 Demospongiae has undoubtedly been the most successful sponge lineage[37]. Furthermore, they have
259 been ecologically more successful being able to transition to freshwater and undergo revolutionary
260 body plan rearrangements, leading to the only known case of carnivory in the phylum[38,39]. Many
261 explanations have been proposed to explain their success. One is that the high diversity of spicule
262 shapes would have been advantageous for structural functions and defence, driving adaptive
263 radiations. Our diversification analyses however highlight a different scenario. While spicules certainly
264 play a role in defence and for structural support, their emergence did not seem to have driven adaptive
265 radiations. If that was the case, we would have expected a diversification event on the branch that
266 leads to the radiation of Heteroscleromorpha. Instead, we retrieve diversification events, consistently
267 across BAMM and Medusa, on the branch that leads to Bubarida and Axinellida (Fig. 3). Both these

268 groups are well nested within Heteroscleromorpha, and spicules were not an innovation specific to
269 them. Furthermore, their spicule types are shared across many other orders in demosponges (Table
270 S5) where we did not identify diversification events. The increase in diversification rates highlighted
271 in these two lineages might be linked to their ecology, however, it would be too speculative to attempt
272 understanding what aspects of their ecology might have driven their radiation.

273 Medusa highlighted a diversification event on the stem Poecilosclerida branch for both the AR
274 and IR timetrees. While Poecilosclerida represents the most speciose demosponge order, with ca.
275 2,488 species described to date (World Porifera Database[37]), have a worldwide distribution, and
276 achieved substantial ecological diversity (evolving also carnivory – family Cladorhizidae), we prefer to
277 maintain a conservative view and consider this result uncertain because it is software-specific. In any
278 case, Poecilosclerida are also members of the spiculated lineage and did not evolve spicules
279 independently. We therefore conclude that while the poecilosclerid evolutionary success might have
280 been linked to the massive expansion of microscleres observed in this clade[40,41], the origin of spicules
281 itself cannot have driven their diversification.

282

283 **An Ediacaran origin of sponges**

284 Irrespective of the fossil calibration strategy used, our divergence time estimates identified the origin
285 of sponges at a time that is significantly younger than previous studies (617.91-581.39 Ma early-
286 middle Ediacaran)[2,4,42]. Our new, younger, divergence times are driven by both a revised
287 geochronology and reinterpretation of the fossil evidence used in establishing calibrations[43]. The
288 earliest fossils that can be assigned to sponges are loosely mineralised siliceous spicules that first occur
289 at the Ediacaran-Cambrian boundary[11–13,44]. Our results indicate that these spicules are uninformative
290 of early sponge evolution. The absence of fossilised spicules before this time does not represent a
291 taphonomic bias due to Neoproterozoic Ocean geochemistry making siliceous spicules difficult to be
292 buried or modified[12], as confirmed by the presence of abundant cherts in the latest Ediacaran[45].
293 Rather, our results indicate that stem- and early crown Porifera lacked spicules (like extant
294 Verongimorpha and Keratosa), and Ediacaran sponges were therefore entirely soft-bodied. The
295 hypothesis that biomineralised sponges were predated by sponges with an organic skeleton has
296 previously been proposed[10] to explain the lack of precambrian sponge fossils. This hypothesis is not
297 supported by the current understanding of siliceous spicule development, as biomineralisation seems
298 to be a fundamental step in spicule biosynthesis (see above), and we therefore suggest that this
299 hypothesis should be considered rejected.

300 Since sponges branch early within the animal phylogeny (irrespective of the current
301 controversy on the relative relationships between sponges and ctenophores in the context of early

302 animal phylogeny[29,46–53]) they are informative regarding early metazoan evolution, and the origin of
303 animal multicellularity. Advocates of a literal reading of the fossil record would suggest that the origin
304 of sponges (and of Metazoa) corresponds closely with the first appearance of siliceous spicules in the
305 fossil record (~543 Ma; latest Ediacaran)[13]. However, molecular timescales derived using relaxed
306 molecular clock methods have dated the origin of sponges (and that of animals) in the Cryogenian (85
307 Ma before the Ediacaran)[2]. Some possible sponge body fossils have previously been suggested to
308 expand the fossil record of sponges into the Cryogenian[9]. However, these records are more
309 speculative than informative, based as they are based on fragmentary remains. Fossilised steranes
310 (24-ipc and 26-mes) from the late Cryogenian (660-635 Ma) have enjoyed a long history of alternative
311 interpretations[54–57]. While originally suggested to indicate the presence of demosponges in the
312 Crypogenian, they have recently been interpreted also to represent diagenetic derivatives of C_{29}
313 sterols from chlorophyte algae[7] (Bobrovskiy et al. 2021). Interpreting these steranes as demosponge
314 biomarkers would have material implications on our evolutionary timescale. However, current
315 ambiguity over their nature implies that, at the least at the time of writing, they cannot be used as
316 calibrations for molecular clock analyses.
317 The absence of siliceous sponge spicules from the fossil record prior to the latest Ediacaran is
318 especially informative since they require no special mechanisms for fossilization[2]. Rather, the absence
319 of Tonian, Cryogenian or deep Ediacaran sponge spicules requires either that sponges had not yet
320 evolved or else that sponge spicules evolved late within the sponge lineage. Our results provide a
321 reconciliation of the sponge fossil record with the molecular timescales of sponge evolution. First, our
322 ASEs show that siliceous spicules emerged relatively late in sponge evolution, in the stem of the
323 spiculated demosponges (heteroscleromorphs). The root of Silicea and of the sponges predate the
324 oldest fossil spicules and our results suggest that early crown sponges existed for ~75–38 million years
325 before the origin of spicules, this interval might diminish with the discovery of increasingly older
326 spicule records. This result finally implies that current estimates of divergence time for Metazoa[4,42]
327 are likely to be overestimated.
328
329 **Material and methods**
330 **Sample collection, RNA extraction, library preparation, Illumina sequencing**
331 Twelve novel sponge specimens were collected for RNA extraction (Supplementary material Table S).
332 Samples were preserved in RNAlater (Thermo Scientific, Waltham, USA) using an overnight incubation
333 at 4°C before long-term storage at -80 °C. Total RNA was extracted with TRIzol (Ambion, Austin, USA)
334 and mRNA purified with a Dynabeads mRNA DIRECT kit (Thermo Scientific, Waltham, USA). The cDNA
335 libraries were constructed with either the kits TruSeq v2 or Scriptseq v2 RNA Library Prep kit (Illumina),

336 according to the manufacturer's instructions, using the maximum quantity of mRNA allowed, which
337 was 50ng – 100ng of starting material. The quality of the libraries was checked with an Agilent
338 TapeStation 2200 system (Agilent Technologies) and the quantity with Qubit™ dsDNA HS Assay kit
339 (ThermoFisher Scientific). The sequencing was conducted with an Illumina NextSeq 500 platform at
340 the Sequencing Facilities of the Natural History Museum of London (Research Core Labs), using a
341 paired-end read strategy (bp length: 2x150 bp).
342
343 **Transcriptome assembly and annotation**
344 Over the 12 novel transcriptomes, 58 published RNA-seq data sets with Sequence Read Archive (SRA)
345 IDs were include, with the final total dataset was composed of 70 proteomes (Table S7). For all
346 transcriptomes assembled, read quality assessment was performed with FastQC[58] with trimming
347 performed with Trimmomatic[59] with the following settings: ILLUMINACLIP:./Adapters.fa:2:30:10
348 LEADING:3 TRAILING:3 SLIDINGWINDOW:4:28 MINLEN:36, with the Adapters.fa file adjusted to
349 include the adapter sequences specific to each read pair. Assembly of the clean paired reads, obtained
350 from Trimmomatic, was performed using Trinity version[60] with the following settings: --
351 normalize_reads –CPU 8 –inchwormcpu 8. Prior to orthology inference, nucleotide sequences were
352 translated using TransDecoder (https://hpc.nih.gov/apps/TransDecoder.html) for a total of 70 species
353 and isoforms were collapsed using CD-HIT[61]. The final total dataset was composed of 70 proteomes
354 (Table S7).
355
356 **Orthology inference**
357 Orthologs were inferred using Orthofinder v. 2.7.1[62], which identified 335,892 orthogroups. Putative
358 paralogous were removed using PhyloTreePruner[63], only orthogroups with at least 90% of the species
359 in the total dataset were retained for further analyses to minimise missing data for a total of 1,468
360 orthogroups retained. Hypervariable regions of the sequences were removed using PREQUAL[64].
361 Orthogroups were aligned using MUSCLE[65]. Final trimming was performed with TrimAl[66] with -auto
362 option for each gene family. After trimming, sequences shorter than 25 AA and with less then 50% of
363 species were removed with Al2Phylo[29]. Single-gene trees were built using IQTree v 1.6.12[67], where a
364 model test was run for each gene tree with the parameters -m MFP -mset LG+F+G, WAG+F+G,
365 JTT+F+G, GTR20 -madd LG+C20+F+G, LG+C10+F+G, LG+C30+F+G, LG+C40+F+G, LG+C50+F+G,
366 LG+C60+F+G, C10, C20, C30, C40, C50, C60, LG4M, LG4X , to allow selecting across compositionally
367 site homogeneous and site heterogeneous models. We further used an in-house developed script
368 (https://github.com/mgiacom/ParaFilter) by Mattia Giacomelli to remove putative hidden paralogs
369 and extremely long branched taxa. Finally, removed gene trees that could not identify the monophyly

370 of sponges or of the outgroup lineages using monophylyl.pl from
371 https://github.com/MaxTelford/Xenacoelomorpha2019. The final dataset was composed of 133
372 genes that were concatenated in a super alignment using the catfasta2phyml.pl script from
373 https://github.com/nylander/catfasta2phyml, for a total length of 103,269 AA.
374
375 **Phylogeny inference**
376 The superalignment was analysed using ML in IQTree2 v2.1.3[68]. Model testing was performed using
377 Model Finder plus (MFP option in IQTree but considering only across-site compositionally
378 homogeneous models)[69]. Across-site compositionally heterogeneous models were not considered
379 because analyses using such models were performed in Phylobayes instead (see below). Model
380 selection identified Q.INSECT+I+G4 model as the best fit across-site compositionally homogeneous
381 models, we used the ultrafast bootstrap (1,000 replicates)[70,71] to estimate support for the nodes in the
382 across-site compositionally homogeneous ML trees. In addition, we ran Phylobayes mpi.1.8[72] under
383 the CAT Poisson model[73] with support values estimated using Posterior Probabilities (PP). We ran two
384 independent chains for over 7,000 generations (Burnin = 1500). Convergence was tested using
385 *Bpcomp* (maxdiff = 0.0018315) and *Tracecomp* (minimal ESS 61 and maximum real_diff=224488)
386 which are part of Phylobayes (See details in table S8). Finally, we used ASTRAL[74] as a coalescent tree
387 reconstruction method of the final 133 gene trees, with default parameters.
388
389 **Timetree inference**
390 Based on the results of ModelFinder analyses performed on the single gene alignments during the
391 gene trees reconstruction described in the orthology inference section, a partitioned dataset was
392 generated (with five partitions – see Supplementary methods for justifications). Prior to timetree
393 inference, we calculated the gradient (i.e., vector of first derivatives of the likelihood function) and
394 the Hessian (i.e., matrix of second derivatives of the likelihood function) for each partition with
395 CODEML, which is part of the PAML package v4.9i[75]. The vector and matrix are necessary to implement
396 approximate maximum likelihood estimation[75](see supplementary information for details).
397 We fixed the tree topology to our inferred Bayesian tree (Fig. S3, S12 and Fig. 1), and
398 constrained the age of 12 nodes representing major sponge clades in our phylogeny (red dots and
399 circles in Fig. 1) based on the fossil record. The oldest fossil spicule was initially used to calibrate the
400 origin of the Spicule-bearing Demospongiae (SDN calibration strategy). We used a uniform prior on
401 the root age with a soft maximum of 609 Ma (pU = 0.025) and a hard minimum of 574 Ma (pL = 1e-
402 300; this small value enables the usage of hard bounds in MCMCtree, pL=0 is not allowed as it would
403 cause numerical underflow). We constrained the age of Eumetazoa with a hard maximum of 573 Ma

404 (pU = 1e-300) and a soft minimum of 561 Ma (pU = 0.025) to avoid truncation issues during the MCMC
405 runs[42]. The age of the other ten calibrated nodes was constrained using heavy-tail Cauchy distributions
406 (i.e., lower-bound calibrations with an offset of p=0.1 or p=0.5, a scale parameter of c=0.5 or c=0.1,
407 and a left tail probability of pL=1e-300). The use of a heavy tailed distribution was preferred as it allows
408 to capture our interpretation of the reliability of the sponge fossil record, which is unlikely to be
409 reliable in deep time because of difficulties for a taxonomic classification given the alteration of
410 diagnostic characters by taphonomic processes. We performed a sensitivity test (SPN strategy) where
411 the oldest siliceous spicule was reassigned to calibrate the node representing the last common sponge
412 ancestor (see also Fig. 1) to investigate what effect, uncertainty in the spicule fossil record, could have
413 on molecular estimates of poriferan divergence times. In brief SDN strategy constrained the spicule
414 bearing Demospongiae (Haploscleromoprha + Heteroscleromoprha) to have a hard minimum at 515
415 Ma, while the SPN strategy constrained the root of Porifera to a minimal age of 515 Ma. Both
416 experiments used a Cauchy distribution specified in the same way (c= 0.5, p = 0.5, and pL=1e-300).
417 The age of 515 used in both the SDN and SPN strategies is based on a loose siliceous spicule from the
418 lower Cambrian (Series 2, Stage 3;) Sirius Passet Biota of North Greenland[30]. A list of all the calibrations
419 used can be found in Supplementary Information. We ran all analyses under both the IR[71,72] and the
420 AR[73,74] relaxed-clock models implemented in the MCMCtree (PAML package v4.9i[75]). Six independent
421 chains for every analysis (SDN+AR, SDN+IR, SPN+AR, SPN+IR) were run with 4,020,000 iterations each.
422 We discarded the first 20,000 as burn-in and subsequently subsampled every 20 iterations. We saved
423 the values sampled for each parameter until reaching a total of 200,000 samples for each chain. As
424 per our MCMC settings, we discarded the first 100,000 collected samples as part of the burn-in phase
425 and, every 100 iterations, we saved the values sampled for each parameter until reaching a total of
426 20,000 samples for each chain. The MCMC settings for the evolutionary model can be found in the
427 supplementary material. We used our in-house pipeline (see
428 https://github.com/MEleonoraRossi/spicules-dating) to (i) filter the six MCMC chains we ran for every
429 data analysis and (ii) generate convergence plots and summary statistics with the chains that passed
430 our quality control checks (see supplementary material and GitHub repository for details).
431
432 **Ancestral state estimation (ASE)**
433 We conducted marginal likelihood ASE in R using the fitmk() and ancr() functions from the phytools
434 package[76]. Character states for the full dataset were retrieved from the literature (Table S9). We coded
435 two discrete characters: (i) presence of mineralised spicules, absent = 0, present = 1; (ii) mineralogy
436 of the spicules, absent = 0, calcite = 1, aragonite = 2, silica = 3. For each character, different transition
437 models were considered: equal rates (ER), symmetrical (SYM) and all rates different (ARD). Note that

438 the symmetrical model is equivalent to the "all rates are different" model for binary characters and
439 was thus not used in these analyses. Observing spicule mineralogy is dependent upon spicule
440 presence. To accommodate the hierarchical nature of this data, we conducted a third ASE analysis in
441 which the characters were amalgamated into a single Structured Markov Model (SMM) equipped with
442 hidden states[77]. We tested 14 different SMMs representing seven patterns of transition rate
443 heterogeneity (Table S10) and two patterns of character correlation: general correlation (SMM_ind)
444 and switch-on dependency (SMM_sw). All ASE analyses were repeated using four trees resulting from
445 four different molecular clock analyses (SDN+AR, SDN+IR, SPN+AR, SPN+IR). Results were summarised
446 using model averaging. Models were weighted using two metrics: (i) Bayesian Information Criterion
447 (BIC); (ii) raw uncertainty of ancestral estimates[78].
448
449 **Diversification Rates through Time and Across Clades**
450 We assembled a dataset of 804 COI sequences from GenBank. The sequences were visualised using
451 Seaview and aligned with MUSCLE v. 3.8.31[65]. The final alignment was 609 bp. We inferred the best-
452 scoring maximum-likelihood (ML) tree with IQTree2 v2.1.3[68]. However, we constrained the analyses
453 using our phylogenomic tree (Fig. 1) as a backbone constraint[25]. Model testing was performed using
454 Model Finder plus (MFP option in IQTree but considering only across-site compositionally
455 homogeneous models)[69], because of the size of the dataset which limited our ability to use complex
456 models. Following the procedure detailed in Álvarez-Carretero et al., 2022[79], we fitted skew-t (ST)
457 distributions to the posterior densities of the divergence times inferred using PAML v4.9i[75] (see
458 Supplementary Method). We selected 13 ST distributions that matched the nodes that had been
459 calibrated prior to timetree inference so that we could use them as prior distributions in the
460 subsequent analyses (Table S11) on the ML topology inferred using the 804 COI sequences. We run 64
461 independent chains with 4,020,000 iterations each. We discarded the first 20,000 as burn-in and
462 subsequently subsampled every 20 iterations. We saved the values sampled for each parameter until
463 reaching a total of 200,000 samples for each chain. Convergence was calculated as explained in the
464 Time tree inference section above (Table S5).
465 Macroevolutionary dynamics of diversification were modelled with the software Bayesian
466 Analysis of Macroevolutionary Mixtures (BAMM) v.2.5.0[26] on the timetree inferred following the
467 procedure described above. We accounted for incomplete taxon sampling by defining a sampling
468 fraction of 5%, which corresponds to the number of species included in the COI dataset compared to
469 the total number of Silicea species accepted. For each order we also calculated the sampling
470 frequences (species sampled/species accepted for the order; data obtained by the World Porifera
471 Database; Table S12). Ten million generations of reversible jump Markov Chain Monte Carlo sampling

472 were run, drawing samples from the posterior every 10,000 generations. For the prior probability of
473 rate shift, we tested values ranging from 0.1 to 50 and chose the value leading to the highest ESS
474 values for LogLikelihood and NumberOfShifts (Table S4). We processed the output data with
475 BAMMtools[80] and, after removing the samples collected during the burn-in process (10% of the
476 samples), we obtained the summary statistics, and plotted the diversification rate over time. To
477 overcome the possible bias introduced by incomplete sampling in diversification analyses and to
478 address the debate around the application of BAMM[26], we confirmed our results using the taxonomic
479 method implemented in MEDUSA[27] where clades are collapsed to terminal lineages of equal ranks.
480 Only diversification events inferred by both methods were deemed reliable.

481 **Data availability**

482 The IDs of genomes and transcriptomes used for the dataset are in table S7 in the supplementary
483 material. The raw reads of the 12 RNA-Seq data generated in this study will be uploaded on the SRA
484 upon acceptance.

485 **Code availability**

486 The in-house pipeline used for the time tree inference can be found on GitHub at
487 https://github.com/MEleonoraRossi/spicules-dating
488 All code used for analysis and figure generation will be released on GitHub at
489 https://github.com/MEleonoraRossi/spicule-evolution upon acceptance.

490 **Ethics statement**

491 The authors declare no competing interests.

492 **Authors' contributions**

493 MER, DP, AR and PJD conceived the study. MER performed the phylogenomic, timetree inference, and
494 diversification event analyses, and wrote the first draft of the paper. DP, PJD and AR edited the paper.
495 MG, NJK, and MER performed orthology inference. JNK provided support for the ASE analyses, SAC
496 provided support and scripts for timetree inference analyses. PC and AS provided some of the fossil
497 calibrations and helped assembling the morphological matrix used in the ASE. ST, VK, AR, and PC took
498 part in the sampling. ST, VK, NJK and MER extracted the RNA and performed library preparations of
499 the samples. All authors have read and wrote the manuscript.

500

501 **Acknowledgments**

502 The authors want to thank Dr. Bruna Plese for her help during the RNA extraction and library
503 preparation. MER is supported by a NERC GW4+ PhD studentship. DP and PJD are supported by the
504 John Templeton Foundation (62220). Please note that the opinions expressed in this publication are
505 those of the author(s) and do not necessarily reflect the views of the John Templeton Foundation, and

the Gordon and Betty Moore Foundation (GBMF9741). DP is supported by a University of Bristol URF fellowship. PJD was supported by a Leverhulme Trust fellowship (RF-2022-167), and a BBSRC grant (BB/T012773/1). DP and PJD were also supported by a NERC-BETR Grant (NE/P013643/1). NJK supported by Rutherford Discovery Fellowship RDF-UOO2001 from the Royal Society of New Zealand. JNK is supported by ERC grant no. 788203 (INNOVATION). AS is supported by Villum Fonden grant no. 679849 and Enbie grant no. 54433.

512 **References**

513

514 1. Gold, D. A. *et al.* Sterol and genomic analyses validate the sponge biomarker hypothesis.
515 *Proc. Natl. Acad. Sci. U.S.A.* **113**, 2684–2689 (2016).
516 2. Sperling, E. A., Robinson, J. M., Pisani, D. & Peterson, K. J. Where's the glass?
517 Biomarkers, molecular clocks, and microRNAs suggest a 200-Myr missing Precambrian
518 fossil record of siliceous sponge spicules: Sponge biomarkers, molecular clocks and
519 microRNAs. *Geobiology* **8**, 24–36 (2010).
520 3. Zumberge, J. A. *et al.* Demosponge steroid biomarker 26-methylstigmastane provides
521 evidence for Neoproterozoic animals. *Nat Ecol Evol* **2**, 1709–1714 (2018).
522 4. Erwin, D. H. *et al.* The Cambrian Conundrum: Early Divergence and Later Ecological
523 Success in the Early History of Animals. *Science* **334**, 1091–1097 (2011).
524 5. Dohrmann, M. & Wörheide, G. Dating early animal evolution using phylogenomic data.
525 *Sci Rep* **7**, 3599 (2017).
526 6. Botting, J. P. & Muir, L. A. Early sponge evolution: A review and phylogenetic framework.
527 *Palaeoworld* **27**, 1–29 (2018).
528 7. Bobrovskiy, I. *et al.* Algal origin of sponge sterane biomarkers negates the oldest
529 evidence for animals in the rock record. *Nature Ecology & Evolution* **5**, 165–168 (2021).
530 8. Zhang, Y., Yuan, X. & Yin, L. Interpreting Late Precambrian Microfossils. *Science* **282**,
531 1783–1783 (1998).
532 9. Maloof, A. C. *et al.* Possible animal-body fossils in pre-Marinoan limestones from South
533 Australia. *Nature Geosci* **3**, 653–659 (2010).
534 10. Yin, Z. *et al.* Sponge grade body fossil with cellular resolution dating 60 Myr before the
535 Cambrian. *Proc. Natl. Acad. Sci. U.S.A.* **112**, (2015).

11. Chang, S., Feng, Q., Clausen, S. & Zhang, L. Sponge spicules from the lower Cambrian in the Yanjiahe Formation, South China: The earliest biomineralizing sponge record. *Palaeogeography, Palaeoclimatology, Palaeoecology* **474**, 36–44 (2017).
12. Tang, Q., Wan, B., Yuan, X., Muscente, A. D. & Xiao, S. Spiculogenesis and biomineralization in early sponge animals. *Nat Commun* **10**, 3348 (2019).
13. Antcliffe, J. B., Callow, R. H. T. & Brasier, M. D. Giving the early fossil record of sponges a squeeze: The early fossil record of sponges. *Biol Rev* **89**, 972–1004 (2014).
14. Borchiellini, C. *et al.* Sponge paraphyly and the origin of Metazoa. *J of Evolutionary Biology* **14**, 171–179 (2001).
15. Chang, S., Zhang, L., Clausen, S., Bottjer, D. J. & Feng, Q. The Ediacaran-Cambrian rise of siliceous sponges and development of modern oceanic ecosystems. *Precambrian Research* **333**, 105438 (2019).
16. Francis, W. R. *et al.* The genome of the reef-building glass sponge *Aphrocallistes vastus* provides insights into silica biomineralization. *R. Soc. open sci.* **10**, 230423 (2023).
17. Dunn, F. S. *et al.* The developmental biology of Charnia and the eumetazoan affinity of the Ediacaran rangeomorphs. *Science advances* **7**, eabe0291 (2021).
18. Yang, C. *et al.* Implications for Ediacaran biological evolution from the ca. 602 Ma Lantian biota in China. *Geology* **50**, 562–566 (2022).
19. Wilby, P. R., Carney, J. N. & Howe, M. P. A rich Ediacaran assemblage from eastern Avalonia: evidence of early widespread diversity in the deep ocean. *Geology* **39**, 655–658 (2011).
20. Noble, S. R. *et al.* U-Pb geochronology and global context of the Charnian Supergroup, UK: constraints on the age of key Ediacaran fossil assemblages. *Bulletin* **127**, 250–265 (2015).

560 21. Thorne, J. L., Kishino, H. & Painter, I. S. Estimating the rate of evolution of the rate of
561 molecular evolution. *Mol Biol Evol* **15**, 1647–1657 (1998).
562 22. Yang, Z. & Rannala, B. Bayesian estimation of species divergence times under a
563 molecular clock using multiple fossil calibrations with soft bounds. *Mol Biol Evol* **23**,
564 212–226 (2006).
565 23. Rannala, B. & Yang, Z. Inferring speciation times under an episodic molecular clock. *Syst*
566 *Biol* **56**, 453–466 (2007).
567 24. Lemey, P., Rambaut, A., Welch, J. J. & Suchard, M. A. Phylogeography takes a relaxed
568 random walk in continuous space and time. *Mol Biol Evol* **27**, 1877–1885 (2010).
569 25. DeBiasse, M. B. *et al.* A cnidarian phylogenomic tree fitted with hundreds of 18S leaves.
570 *bioRxiv* 2022–10 (2022).
571 26. Rabosky, D. L. Automatic Detection of Key Innovations, Rate Shifts, and Diversity-
572 Dependence on Phylogenetic Trees. *PLOS ONE* **9**, e89543 (2014).
573 27. Alfaro, M. E. *et al.* Nine exceptional radiations plus high turnover explain species
574 diversity in jawed vertebrates. *Proceedings of the National Academy of Sciences* **106**,
575 13410–13414 (2009).
576 28. Lavrov, D. V. *et al. Phylomitogenomics Bolsters the High-Level Classification of*
577 *Demospongiae (Phylum Porifera)*.
578 http://biorxiv.org/lookup/doi/10.1101/2023.06.04.543631 (2023)
579 doi:10.1101/2023.06.04.543631.
580 29. Simion, P. *et al.* A Large and Consistent Phylogenomic Dataset Supports Sponges as the
581 Sister Group to All Other Animals. *Current Biology* **27**, 958–967 (2017).
582 30. Botting, J. P., Cárdenas, P. & Peel, J. S. A crown-group demosponge from the early
583 Cambrian Sirius Passet Biota, North Greenland. *Palaeontology* **58**, 35–43 (2015).

31. Voigt, O. *et al.* Spicule formation in calcareous sponges: Coordinated expression of biomineralization genes and spicule-type specific genes. *Sci Rep* **7**, 45658 (2017).
32. Riesgo, A., Maldonado, M., López-Legentil, S. & Giribet, G. A Proposal for the Evolution of Cathepsin and Silicatein in Sponges. *J Mol Evol* **80**, 278–291 (2015).
33. Shimizu, K. *et al.* Silica-associated proteins from hexactinellid sponges support an alternative evolutionary scenario for biomineralization in Porifera. *Nature Communications* **15**, 181 (2024).
34. Cha, J. N. *et al.* Silicatein filaments and subunits from a marine sponge direct the polymerization of silica and silicones in vitro. *Proceedings of the National Academy of Sciences* **96**, 361–365 (1999).
35. Shimizu, K., Cha, J., Stucky, G. D. & Morse, D. E. Silicatein α: Cathepsin L-like protein in sponge biosilica. *Proceedings of the National Academy of Sciences* **95**, 6234–6238 (1998).
36. Müller, W. E. G. *et al.* Analysis of the axial filament in spicules of the demosponge Geodia cydonium: Different silicatein composition in microscleres (asters) and megascleres (oxeas and triaenes). *European Journal of Cell Biology* **86**, 473–487 (2007).
37. de Voogd, N. *et al.* World Porifera Database. Accessed at https://www.marinespecies.org/porifera on yyyy-mm-dd. VLIZ https://doi.org/10.14284/359 (2023).
38. Hestetun, J. T. *et al.* The systematics of carnivorous sponges. *Mol Phylogenet Evol* **94**, 327–345 (2016).
39. Vacelet, J. & Boury-Esnault, N. Carnivorous sponges. *Nature* **373**, 333–335 (1995).
40. Łukowiak, M. *et al.* The terminology of sponge spicules. *Journal of Morphology* **283**, 1517–1545 (2022).

608 41. Morrow, C. & Cárdenas, P. Proposal for a revised classification of the Demospongiae
609 (Porifera). *Front Zool* **12**, 7 (2015).
610 42. dos Reis, M. *et al.* Uncertainty in the Timing of Origin of Animals and the Limits of
611 Precision in Molecular Timescales. *Curr Biol* **25**, 2939–2950 (2015).
612 43. Carlisle E., Yin Z., Pisani D. and Donoghue PCJ. Ediacaran origin and Ediacaran-Cambrian
613 diversification of Metazoa.
614 44. Chen, C. *et al.* New sponge spicules from the Ediacaran-Cambrian transition in deep-
615 water facies of South China. *Palaeogeography, Palaeoclimatology, Palaeoecology* **627**,
616 111714 (2023).
617 45. Muscente, A., Michel, F. M., Dale, J. G. & Xiao, S. Assessing the veracity of Precambrian
618 'sponge'fossils using in situ nanoscale analytical techniques. *Precambrian Research* **263**,
619 142–156 (2015).
620 46. Dunn, C. W. *et al.* Broad phylogenomic sampling improves resolution of the animal tree
621 of life. *Nature* **452**, 745–749 (2008).
622 47. Feuda, R. *et al.* Improved modeling of compositional heterogeneity supports sponges as
623 sister to all other animals. *Current Biology* **27**, 3864–3870 (2017).
624 48. Kapli, P. & Telford, M. J. Topology-dependent asymmetry in systematic errors affects
625 phylogenetic placement of Ctenophora and Xenacoelomorpha. *Science Advances* **6**,
626 eabc5162 (2020).
627 49. Li, Y., Shen, X.-X., Evans, B., Dunn, C. W. & Rokas, A. Rooting the Animal Tree of Life.
628 *Molecular Biology and Evolution* **38**, 4322–4333 (2021).
629 50. Philippe, H. *et al.* Phylogenomics Revives Traditional Views on Deep Animal
630 Relationships. *Current Biology* **19**, 706–712 (2009).
631 51. Pisani, D. *et al.* Genomic data do not support comb jellies as the sister group to all other

632 animals. *Proceedings of the National Academy of Sciences* **112**, 15402–15407 (2015).
633 52. Whelan, N. V. *et al.* Ctenophore relationships and their placement as the sister group to
634 all other animals. *Nat Ecol Evol* **1**, 1737–1746 (2017).
635 53. Whelan, N. V., Kocot, K. M. & Halanych, K. M. Employing Phylogenomics to Resolve the
636 Relationships among Cnidarians, Ctenophores, Sponges, Placozoans, and Bilaterians.
637 *Integrative and Comparative Biology* **55**, 1084–1095 (2015).
638 54. Antcliffe, J. B. Questioning the evidence of organic compounds called sponge
639 biomarkers. *Palaeontology* n/a-n/a (2013) doi:10.1111/pala.12030.
640 55. Nettersheim, B. J. *et al.* Putative sponge biomarkers in unicellular Rhizaria question an
641 early rise of animals. *Nat Ecol Evol* **3**, 577–581 (2019).
642 56. van Maldegem, L. M. *et al.* Geological alteration of Precambrian steroids mimics early
643 animal signatures. *Nature Ecology & Evolution* **5**, 169–173 (2021).
644 57. Love, G. D. *et al.* Sources of C30 steroid biomarkers in Neoproterozoic–Cambrian rocks
645 and oils. *Nature ecology & evolution* **4**, 34–36 (2020).
646 58. Andrews, S. FastQC: a quality control tool for high throughput sequence data. (2010).
647 59. Bolger, A. M., Lohse, M. & Usadel, B. Trimmomatic: a flexible trimmer for Illumina
648 sequence data. *Bioinformatics* **30**, 2114–2120 (2014).
649 60. Grabherr, M. G. *et al.* Full-length transcriptome assembly from RNA-Seq data without a
650 reference genome. *Nature biotechnology* **29**, 644–652 (2011).
651 61. Fu, L., Niu, B., Zhu, Z., Wu, S. & Li, W. CD-HIT: accelerated for clustering the next-
652 generation sequencing data. *Bioinformatics* **28**, 3150–3152 (2012).
653 62. Emms, D. M. & Kelly, S. OrthoFinder2: fast and accurate phylogenomic orthology
654 analysis from gene sequences. *BioRxiv* **466201**, (2018).
655 63. Kocot, K. M., Citarella, M. R., Moroz, L. L. & Halanych, K. M. PhyloTreePruner: A

656 Phylogenetic Tree-Based Approach for selection of Orthologous sequences for
657 phylogenomics. *Evol Bioinform Online* **9**, EBO.S12813 (2013).
658 64. Whelan, S., Irisarri, I. & Burki, F. PREQUAL: detecting non-homologous characters in sets
659 of unaligned homologous sequences. *Bioinformatics* (2018)
660 doi:10.1093/bioinformatics/bty448.
661 65. Edgar, R. C. MUSCLE: multiple sequence alignment with high accuracy and high
662 throughput. *Nucleic Acids Research* **32**, 1792–1797 (2004).
663 66. Capella-Gutiérrez, S., Silla-Martínez, J. M. & Gabaldón, T. trimAl: a tool for automated
664 alignment trimming in large-scale phylogenetic analyses. *Bioinformatics* **25**, 1972–1973
665 (2009).
666 67. Nguyen, L.-T., Schmidt, H. A., von Haeseler, A. & Minh, B. Q. IQ-TREE: A Fast and
667 Effective Stochastic Algorithm for Estimating Maximum-Likelihood Phylogenies.
668 *Molecular Biology and Evolution* **32**, 268–274 (2015).
669 68. Minh, B. Q. *et al.* IQ-TREE 2: New Models and Efficient Methods for Phylogenetic
670 Inference in the Genomic Era. *Molecular Biology and Evolution* **37**, 1530–1534 (2020).
671 69. Kalyaanamoorthy, S., Minh, B. Q., Wong, T. K. F., von Haeseler, A. & Jermiin, L. S.
672 ModelFinder: fast model selection for accurate phylogenetic estimates. *Nature Methods*
673 **14**, 587–589 (2017).
674 70. Hoang, D. T., Chernomor, O., Von Haeseler, A., Minh, B. Q. & Vinh, L. S. UFBoot2:
675 improving the ultrafast bootstrap approximation. *Molecular biology and evolution* **35**,
676 518–522 (2018).
677 71. Minh, B. Q., Nguyen, M. A. T. & Von Haeseler, A. Ultrafast approximation for
678 phylogenetic bootstrap. *Molecular biology and evolution* **30**, 1188–1195 (2013).
679 72. Lartillot, N., Rodrigue, N., Stubbs, D. & Richer, J. PhyloBayes MPI: Phylogenetic

680 Reconstruction with Infinite Mixtures of Profiles in a Parallel Environment. *Systematic*
681 *Biology* **62**, 611–615 (2013).
682 73. Lartillot, N. & Philippe, H. A Bayesian Mixture Model for Across-Site Heterogeneities in
683 the Amino-Acid Replacement Process. *Molecular Biology and Evolution* **21**, 1095–1109
684 (2004).
685 74. Mirarab, S. *et al.* ASTRAL: genome-scale coalescent-based species tree estimation.
686 *Bioinformatics* **30**, i541–i548 (2014).
687 75. Yang, Z. PAML 4: Phylogenetic Analysis by Maximum Likelihood. *Molecular Biology and*
688 *Evolution* **24**, 1586–1591 (2007).
689 76. Revell, L. J. phytools: an R package for phylogenetic comparative biology (and other
690 things). *Methods in Ecology and Evolution* **3**, 217–223 (2012).
691 77. Tarasov, S. Integration of Anatomy Ontologies and Evo-Devo Using Structured Markov
692 Models Suggests a New Framework for Modeling Discrete Phenotypic Traits. *Systematic*
693 *Biology* **68**, 698–716 (2019).
694 78. Keating, J. N. What is the best method for estimating ancestral states from discrete
695 characters? 2023.08.31.555762 Preprint at https://doi.org/10.1101/2023.08.31.555762
696 (2023).
697 79. Álvarez-Carretero, S. *et al.* A species-level timeline of mammal evolution integrating
698 phylogenomic data. *Nature* **602**, 263–267 (2022).
699 80. Rabosky, D. L. *et al.* BAMMtools: an R package for the analysis of evolutionary dynamics
700 on phylogenetic trees. *Methods in Ecology and Evolution* **5**, 701–707 (2014).
701
702
703
704

705 **MAIN FIGURES**

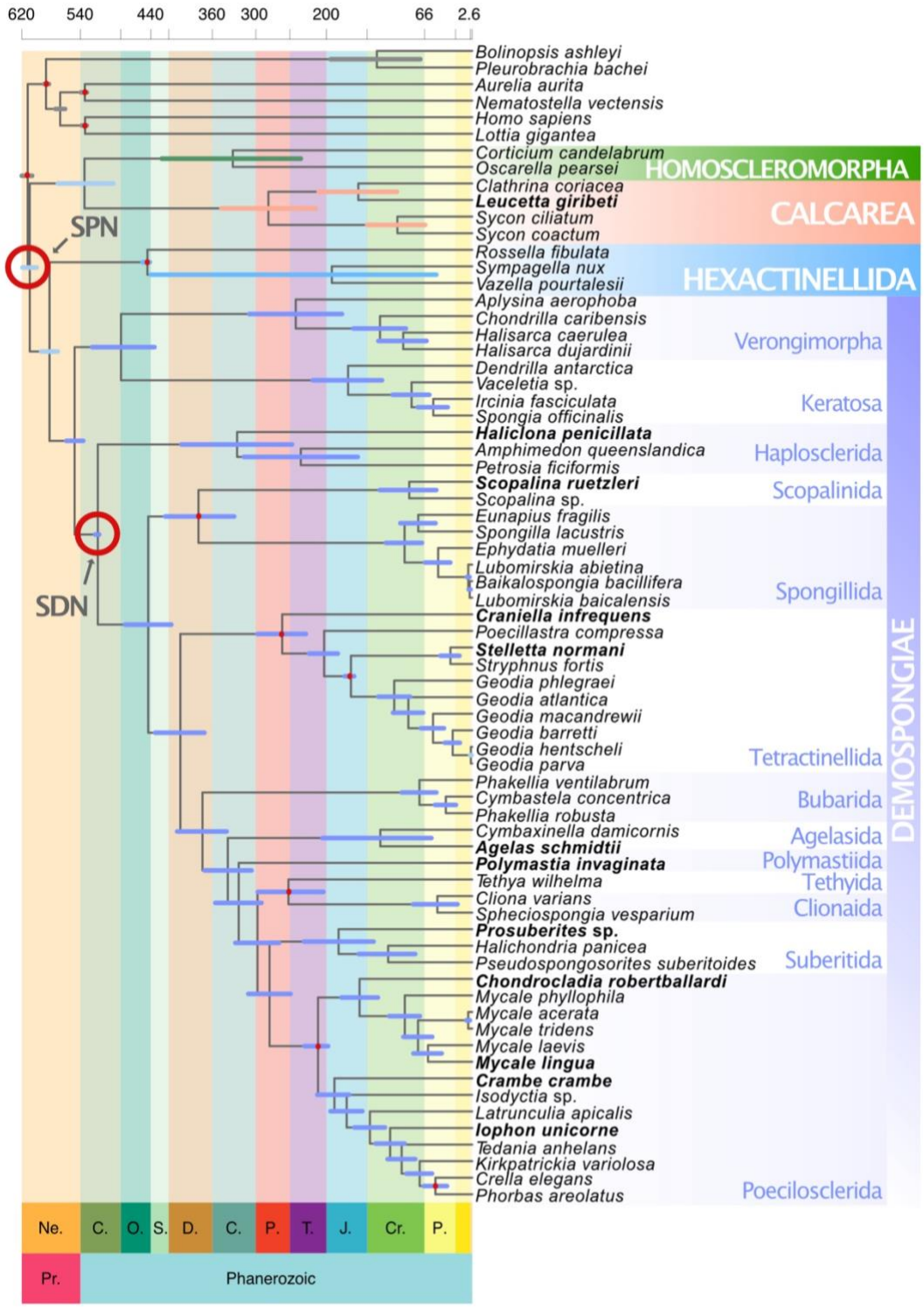

706

707 **Figure 1** Porifera time-tree with posterior estimates using the Spicule-bearing Demospongiae (SDN)
708 calibration strategy (red circle) and the ILN model in MCMCTree. Blue bars on nodes represent the
709 95% HPD. Red circles represent the two mutually exclusive calibrations strategies Spiculated Porifera
710 Node (SPN) and SDN. Full red dots represent calibrations in both strategies. Species in bold were
711 sequences in the framework of this study. Time scale on x-axis in hundreds of millions of years.

Abbreviation on the scale bar stands for Ne, Neoproterozoic; C, Cambrian; O, Ordovician; S, Silurian; D, Devonian; C, Carboniferous; P, Permian; Tr, Triassic; J, Jurassic; K, Cretaceous; Pe, Paleogene.

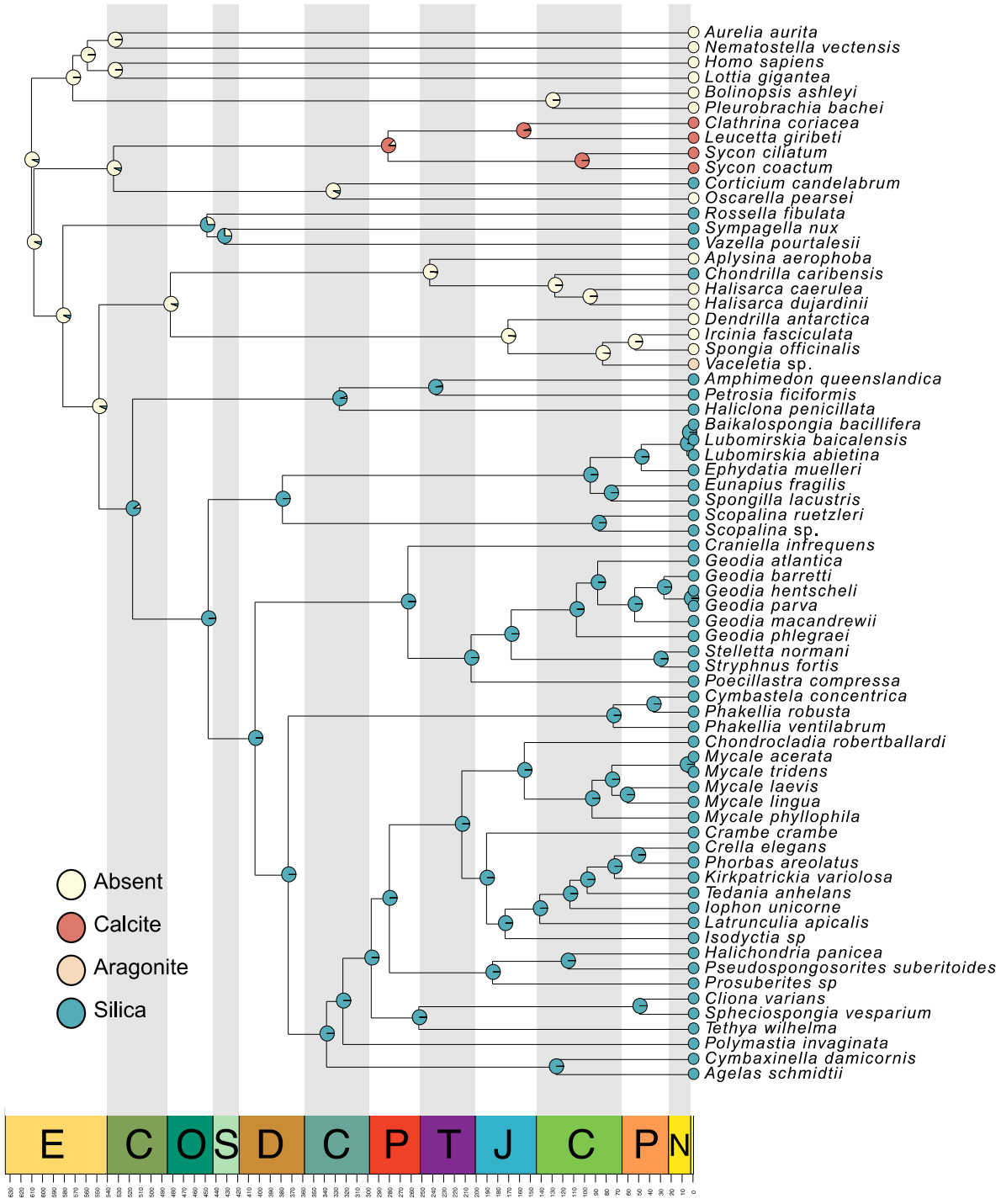

Figure 2 Ancestral state estimations of spicule evolution obtained using the time-tree with the SDN calibration strategy and the SMM combining the presence/absence of spicules and their mineralogy. Cream dots indicate absence of spicules, blue stands for siliceous spicules, red for calcareous spicules, and light orange stands for aragonite.

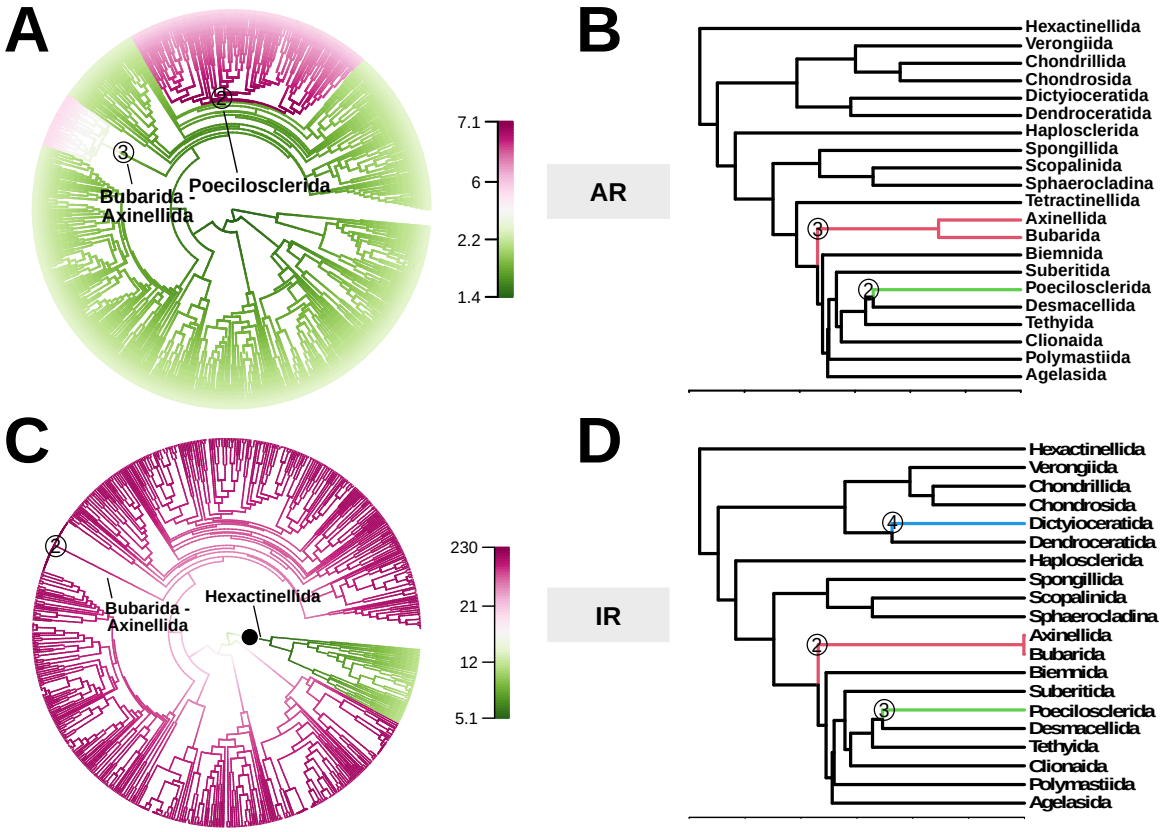

Figure 3 Rate diversification tests. Grey dots with numbers correspond to the shift highlighted by both Medusa and BAMM analyses, the same number is reported when the same shift corresponds on both topologies. A) BAMM results for the COI timetree inferred with the AR model. The two shifts highlighted are on the branches of Bubarida + Axinellida (3), and Poecilosclerida (2). B) Medusa results for the subsampled topology obtained with the AR molecular clock model. C) BAMM results for the COI timetree inferred with the IR molecular clock model. The two shifts highlighted are on the branches of Bubarida + Axinellida (2) and Hexacintellida (black full dot). D) Medusa results for the subsampled topology obtained with the IR molecular clock model which highlights diversification rates in Axinellida+ Bubarida(2), Poecilosclerida (3), and Dyctioceratida (4).

TABLES

Table 1 Summary of mean time estimates for all calibration strategies obtained with MCMCTree for the classes of Porifera, the Silicea clade, and Heteroscleromorpha. Full details can be found in Table S3-S4.

Nodes	SDN AR time estimates	SPN AR time estimates	SDN ILN time estimates	SDN ILN time estimates

Porifera	603.79-582.68	594.59-578.79	615.32-601.3	610.68-590.34
Silicea	577.48-561.72	567.69-551.55	591.32-570.3	575.87-542.68
Demospongiae	549.57-538.18	535.02-503.38	559.17-536.53	519.67-462.67
Hexactinellida	454.92-445.07	443.89-422.5	457.3-445.09	454.99-445.07
Calcarea	473.24-163.27	460.38-157.52	351.7-213.89	337.36-207.53
Homoscleromorpha	540.28-435.36	535.63-420.18	429.15-228.57	421.58-224.87
Heteroscleromorpha	521.97-515.05	500.69-455.96	520.81-515.04	454.95-396.53